

Article

Curcumin Incorporation into Zn₃Al Layered Double Hydroxides—Preparation, Characterization and Curcumin Release

Octavian D. Pavel ¹, Ariana Șerban ^{1,2}, Rodica Zăvoianu ^{1,*}, Elena Bacalum ¹ and Ruxandra Bîrjega ³

¹ Biochemistry and Catalysis, Department of Organic Chemistry, Faculty of Chemistry, University of Bucharest, 030018 Bucharest, Romania; octavian.pavel@chimie.unibuc.ro (O.D.P.); ariana.serban@infim.ro (A.Ș.); elena.bacalum@gmail.com (E.B.)

² National Institute for Materials Physics, 077125 Măgurele, Romania

³ National Institute for Lasers, Plasma and Radiation Physics-INFLPR, 077125 Măgurele, Romania; ruxandra.birjega@inflpr.ro

* Correspondence: rodica.zavoianu@chimie.unibuc.ro; Tel.: +40-746-171-699

Received: 29 February 2020; Accepted: 25 March 2020; Published: 26 March 2020



Abstract: Curcumin (CR) is a natural antioxidant compound extracted from *Curcuma longa* (turmeric). Until now, researches related to the incorporation of CR into layered double hydroxides (LDHs) were focused only on hybrid structures based on a Mg₃Al-LDH matrix. Our studies were extended towards the incorporation of CR in another type of LDH-matrix (Zn₃Al-LDH) which could have an even more prolific effect on the antioxidant activity due to the presence of Zn. Four CR-modified Zn₃Al-LDH solids were synthesized, e.g., PZn₃Al-CR(Aq), PZn₃Al-CR(Et), RZn₃Al-CR(Aq) and RZn₃Al-CR(Et) (molar ratio CR/Al = 1/10, where P and R stand for the preparation method (P = precipitation, R = reconstruction), while (Aq) and (Et) indicate the type of CR solution, aqueous or ethanolic, respectively). The samples were characterized by XRD, Attenuated Total Reflectance Fourier Transformed IR (ATR-FTIR) and diffuse reflectance (DR)-UV-Vis techniques and the CR-release was investigated in buffer solutions at different pH values (1, 2, 5, 7 and 8). XRD results indicated a layered structure for PZn₃Al-CR(Aq), PZn₃Al-CR(Et), RZn₃Al-CR(Aq) impurified with ZnO, while RZn₃Al-CR(Et) contained ZnO nano-particles as the main crystalline phase. For all samples, CR-release revealed a decreasing tendency towards the pH increase, and higher values were obtained for RZn₃Al-CR(Et) and PZn₃Al-CR(Et) (e.g., 45% and 25%, respectively at pH 1).

Keywords: layered double hydroxides; reconstruction; curcumin; drug release

1. Introduction

Turmeric (*Curcuma longa*) is a notorious spice, highly esteemed not only by the scientific world but also by gastronomes as it is the primary source of curcumin (CR) or (1E,6E)-1,7-bis(4-hydroxy-3-methoxyphenyl)hepta-1,6-diene-3,5-dione, a renowned natural antioxidant polyphenol that can scavenge free radicals undergoing electron transfer or abstract H-atoms either from the phenolic OH groups or the CH₂ group of the β-diketone moiety [1–4]. Depending on the chemical environment, CR, an α,β-unsaturated β-diketone can adopt two different conformations, either the diketonic form or the enolic one (Figure 1) [2].

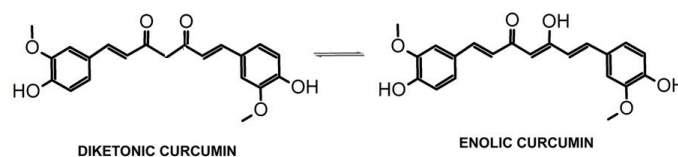


Figure 1. Keto-enolic tautomerization of curcumin.

The antioxidant activity of this natural polyphenol is a controversy for the scientific world. Some consider that the enol tautomer characterized by a better conjugation between the two aromatic rings containing the phenolic OH groups holds the main responsibility for the presence of the antioxidant activity highlighted as an inhibition of superoxide radicals, hydrogen peroxide and nitric oxide radical [3,5], while others acknowledge better the keto form due to its existence in slightly acidic media [6,7]. It was also suggested that the presence of CR accelerates the processes catalyzed by several antioxidant enzymes such as catalase, superoxide dismutase (SOD), glutathione peroxidase (GPx) and heme oxygenase-1 (OH-1) [5]. Since this compound has low solubility in water at neutral pH, its absorption and bioavailability are poor. In addition to that, it has also reduced stability towards oxidation, light, alkalinity, enzymes and heat. Therefore in order to increase its pharmacological effectiveness, the latest researches were focused on improving the bioavailability, chemical and photochemical stability of CR using different methods such as: conjugation with cyclodextrin, β -diglucoside, α S1-Casein, β -Lactoglobulin [8–11], encapsulation in nanoparticles of biocompatible polymers, exosomes, lipid nanoparticles, dextrin nanogels, dendrimers, metal oxide nanoparticles [12–18], complexation with multivalent metal cations [19,20].

Layered double hydroxides are substances belonging to the class of anionic clays, having the general formula $[M^{2+}_{1-x}M^{3+}_x(OH)_2]^{x+}[A^{n-}_{x/n}]^{x-} \cdot mH_2O$ (M^{2+} and M^{3+} are metal cations that can adopt an octahedral arrangement similar to the one adopted by Mg^{2+} in brucite, A^{n-} is a compensation anion, x is a value in the range of 0.2–0.33 and m is the number of water molecules) [21]. The presence of the trivalent cations leads to an excess of positive charge in the brucite-type layer which is compensated by anions A^{n-} , which are located in the interlayer region along with the crystallization water molecules. Even though the hydrotalcite ($Mg_6Al_2(OH)_{16}CO_3 \cdot 4H_2O$) is the most renowned representative of this type of materials, there are also other natural occurring layered double hydroxide (LDH) compounds such as meixnerite ($Mg_6Al_2(OH)_{18} \cdot 4H_2O$), zaccagnaite ($Zn_4Al_2(OH)_{12}[CO_3] \cdot 3H_2O$) and pyroaurite ($Mg_6Fe_2(OH)_{16}CO_3 \cdot 4.5H_2O$). Structurally, these solids consist of positively charged brucite-type layers with balancing anions and water molecules in the interlayer space [21]. Despite the fact that there is a scarce spreading of LDHs in the earth crust, several laboratory methods for their obtaining were developed: co-precipitation at a variable or constant pH, under low or high supersaturation conditions, sol-gel, hydrothermal and mechanochemical synthesis [21–24]. An interesting feature of the LDHs is the so-called “memory effect” which allows the reconstruction of the layered structure when the mixed oxide obtained by thermal decomposition of an LDH precursor at temperatures lower than 550 °C is immersed in an aqueous solution containing the desired compensation anion which can be either inorganic or organic [21,22]. LDH compounds are considered to have low toxicity, good biocompatibility and a buffering action when immersed in aqueous solutions, therefore they were also utilized in medical formulations (such as the antacid TALCID®), for ibuprofen slow release, in colon-targeted drug-delivery, for anticancer methotrexate delivery [25–28] and as matrices for bioinorganic hybrid materials [29–31]. Due to their structure LDHs compounds have anion exchange properties and are frequently utilized as anion exchangers and adsorbents. The insertion of organic anions in the LDH can be performed by ionic exchange, co-precipitation or reconstruction. However, the process is more difficult due to the poorer aqueous solubility of the organic species [22,27,32]. Recently, Kottegoda and coworkers showed that the inhibitory activity against several microbial species (e.g., *Candida albicans*, *Candida dubliniensis*, *Pseudomonas aeruginosa*, *Escherichia coli* and *Staphylococcus aureus*) can be enhanced by CR encapsulation into an inorganic host, namely a layered double hydroxide (LDH) containing Mg and Al as metal cations [33–35].

Considering this state of the art, the present contribution aims to extend the studies towards the incorporation of CR in another type of LDH-matrix, namely Zn₃Al-LDH that is less basic than Mg₃Al-LDH and could bring its own contribution in increasing the antioxidant activity due to the presence of Zn which is known for its antiseptic properties [36]. The target of this study was to choose the modality for obtaining the solid with the best capacity to incorporate CR during synthesis and the best ability to release it in vitro under controlled buffer conditions. Therefore, for the synthesis of CR-containing Zn₃Al-LDH, two different methods were applied: (i) direct co-precipitation (P) and (ii) reconstruction (R) of the LDH in the presence of CR, which was added either as an aqueous alkaline solution (Aq) or as an ethanolic solution (Et). Depending on the applied preparation protocol, the names of the synthesized solids were abbreviated as PZn₃Al-CR(Aq), PZn₃Al-CR(Et), RZn₃Al-CR(Aq) and RZn₃Al-CR(Et). The structural characterization of the samples was performed using X-ray diffraction (XRD), attenuated total reflectance Fourier transformed infrared spectroscopy (ATR-FTIR) and diffuse reflectance UV-Vis spectroscopy (DR-UV-Vis). The release of CR from the solids was investigated in buffer solutions at different pH values (1, 2, 5, 7 and 8) and the spent solid samples recovered after 24 h were also characterized by ATR-FTIR and DR-UV-Vis. Based on the obtained results, the sample allowing the highest CR-release was selected for further antimicrobial activity tests which are going to be the subject of a future publication.

2. Materials and Methods

Curcumin (CR) from Sigma-Aldrich, Zn(NO₃)₂•2H₂O, Al(NO₃)₃•9H₂O, NaOH and Na₂CO₃ from Merck were utilized as raw materials for the synthesis of the CR-functionalized LDHs. Absolute ethanol from Fluka and deionized water were used as solvents. Certified SUPELCO buffer solutions of pH 1 (glycine, sodium chloride, hydrochloric acid), pH 2 (citric acid, sodium hydroxide, hydrochloric acid), pH 5 (citric acid, sodium hydroxide) and pH 7 (potassium dihydrogen phosphate/di-sodium hydrogen phosphate) were purchased from Merck, while the certified Fischer Chemical buffer solution of pH 8 (potassium dihydrogen phosphate/sodium hydroxide) was purchased from Fischer Scientific.

A pristine Zn₃Al-LDH with interlayer carbonate anion was prepared by co-precipitation at pH 9 using 160 mL of a metal nitrates Zn(NO₃)₂•6H₂O, Al(NO₃)₃•9H₂O aqueous solution (1.5 M, molar ratio Zn/Al = 3/1) and 160 mL of an aqueous solution containing Na₂CO₃ and NaOH 160 mL (1 M concentration of Na₂CO₃, 2.5 M concentration of NaOH) for pH adjustment. The resulting gel was aged 18 h at 50 °C. The solid recovered by filtration was washed with deionized water until the conductivity of the wastewater was lower than 100 µS/cm and dried at 90 °C for 24 h and the reference material Zn₃Al-LDH was finally obtained.

The preparation of CR-containing Zn₃Al-LDH was performed using always an amount of CR corresponding to a molar ratio CR/Al = 1/10. For the synthesis by co-precipitation at pH 9 the above-mentioned amount of metal nitrates in aqueous solution were utilized and the pH was adjusted with an aqueous solution of NaOH (2.5 M). Two samples, e.g., PZn₃Al-CR(Aq) and PZn₃Al-CR(Et), were obtained following this procedure since CR was added either as an aqueous alkaline solution (Aq) or as an ethanolic solution (Et). Then, 100 mL of deionized water were poured in the reactor before starting the precipitation of PZn₃Al-CR(Aq) by concomitantly adding the metal nitrates solution and the alkaline solution containing CR under vigorous stirring (350 rot/min). For the obtaining of PZn₃Al-CR(Et), 100 mL of CR ethanolic solution were first added in the reactor and then the precipitation took place by concomitantly adding the solutions containing the metal nitrates and the NaOH under similar conditions of stirring. The flowchart for these preparations is presented in Figure 2. The aging of the precipitates was performed under an inert atmosphere (He flow 10 mL/min).

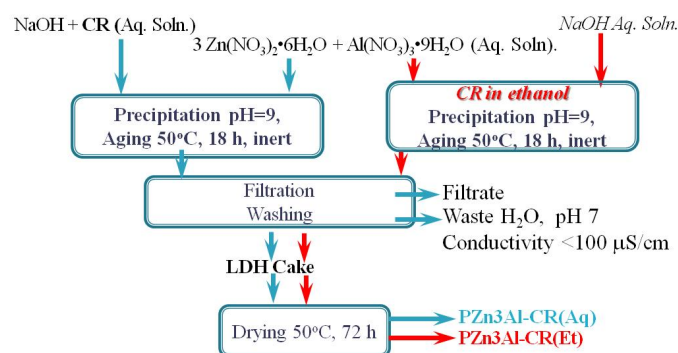


Figure 2. Flowchart for the preparation of curcumin (CR)-containing Zn_3Al -layered double hydroxide (LDH) by co-precipitation.

For the preparations performed by reconstruction a mixed oxide called CZn_3Al obtained by the thermal decomposition of the pristine $\text{Zn}_3\text{Al-LDH}$ at 460 °C during 18 h was utilized as raw material. The reconstructions were performed in brown glass vessels at 25 °C by contacting CZn_3Al powder with a CR-containing solution under magnetic stirring and inert atmosphere (He 1atm) during 24 h. Two CR-containing solutions were prepared, an alkaline aqueous solution containing CR and NaOH at a concentration of 4×10^{-3} M, and an ethanolic solution containing 4×10^{-3} M CR. Depending on the type of CR-solution utilized for reconstruction, two solid samples were obtained, e.g., $\text{RZn}_3\text{Al-CR(Aq)}$ and $\text{RZn}_3\text{Al-CR(Et)}$, respectively. The washing of the recovered solids was performed with deionized water for $\text{RZn}_3\text{Al-CR(Aq)}$, and with ethanol for $\text{RZn}_3\text{Al-CR(Et)}$. The flowchart for these preparations is presented in Figure 3.

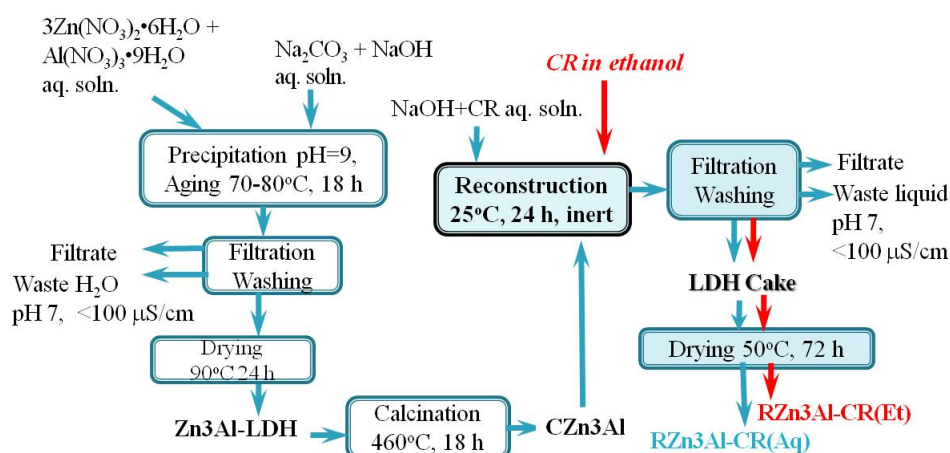


Figure 3. Flowchart for the preparation of CR-containing $\text{Zn}_3\text{Al-LDH}$ by reconstruction.

The content of Zn and Al in the solids was determined by atomic absorption spectrometry (AAS) using a Thermo Elemental Solar AAS apparatus, while the content of CR in the solid samples was calculated based on the determination of total organic carbon (TOC) content using HiPerTOC–Thermo carbon analyzer according to a previously described protocol [37]. The value of TOC was calculated as the difference between total carbon (TC content obtained by UV-persulfate oxidation of the samples) and total inorganic carbon (TIC content obtained by mineralization of the samples with HNO_3 to convert the bicarbonate and carbonate ions to CO_2).

The XRD patterns of the samples were recorded on PANalytical MPD system using Ni-filtered CuK_α radiation ($\lambda = 1.5418 \text{ \AA}$), with a scan step of 0.02° and a counting time of 20 s per step, for 2θ ranging between 5 and 70° . The average crystallite size (D) of the different phases in the samples was determined using the Scherrer formula applied to particular reflections/crystallographic directions.

The characterization of the samples by infrared spectroscopy was performed using a JASCO 4700 FT-IR spectrophotometer equipped with ATR PRO ONE Single-reflection ATR accessory and monolithic diamond crystal on the 4000–400 cm^{-1} domain at 128 scans and a resolution of 4 cm^{-1} .

Shimadzu 3600 UV–Vis NIR spectrometer equipped with an integration sphere was utilized for recording the DR-UV–Vis spectra of the solids in the range of 200–800 nm, using BaSO_4 as white reference.

In vitro CR release studies were performed in dark brown bottles where 0.5 g of solid sample were contacted with 50 mL of the adequate buffer solution (pH 1, pH 2, pH 5, pH 7 and pH 8) at 25 °C during 24 h under mild stirring (100 rot/min). The amount of released CR was determined by UV–Vis spectrometry using a JASCO V650 UV–Vis double-beam spectrophotometer with a photomultiplier tube detector. Liquid samples were withdrawn from the bottles hourly in the first four hours and finally after 24 h and their absorption spectra were recorded in the range 350–550 nm against the corresponding buffer solution as blank. The concentration of CR in the solution was calculated with Equations (1)–(3):

$$C_{\text{CRsolution}} = A_{423\text{nm}}/8153.5 [\text{mol/L}] = A_{423\text{nm}}/22.13 [\text{g/L}] \quad (1)$$

$$m_{\text{CR in 50 mL solution}} = C_{\text{CRsolution}}/20 [\text{g}] \quad (2)$$

$$\% \text{CR}_{\text{released}} = m_{\text{CR in 50 mL solution}} \times 100 / (m_{\text{solid}} \times C_{\text{CR in the solid (see Table 1)}}) \quad (3)$$

Table 1. Chemical composition of the solids.

Sample	Zn (wt. %)	Al (wt. %)	CO_3 (wt. %) ¹	CR (wt. %) ²	H_2O (wt. %) ³	Molar Ratio	
						Zn/Al	CR/Al
Zn3Al-LDH	46.2	6.4	7.1	0	8.5	2.97	0
PZn3Al-CR(Aq)	49.9	7.2	2.8	12.1	8.9	2.86	1/8.5
PZn3Al-CR(Et)	48.1	6.8	1.7	9.3	8.8	2.90	1/10
RZn3Al-CR(Aq)	51.1	7.2	1.2	10.0	5.6	2.91	1/9.9
RZn3Al-CR(Et)	60.3	8.4	0.2	11.5	2.9	2.97	1/9.9

¹ Calculated from TIC (wt. %) values CO_3 (wt. %) = TIC/0.2; ² Calculated from TOC (wt. %) values: CR (wt. %) = TOC (wt. %)/0.684; ³ H_2O calculated considering the loss of weight in the temperature range 105–200 °C [21].

3. Results

3.1. Characterization of the Curcumin Containing Zn3Al-LDHs

3.1.1. Chemical Composition

The results obtained by AAS for the determination of Zn and Al content and the content of carbonate and CR in the samples calculated from the determination of the carbon content (see Table 1) showed that the molar ratios Zn/Al and CR/Al were very close to 3/1 and 1/10, respectively (calculated from the amounts introduced in the synthesis mixture) for all the samples besides PZn3Al-CR(Aq) which showed lower values. The higher concentrations of Zn and Al in RZn3Al-CR(Et) are explained by the lower value of the H_2O concentration in this sample.

3.1.2. XRD Characterization of CR Functionalized Zn3Al-LDH Samples

The XRD patterns of the CR-loaded powders prepared by both direct precipitation and reconstruction are presented in Figure 4. The XRD patterns of curcumin-loaded powders are compared with those of the curcumin free powders obtained either by precipitation (Zn3Al-LDH) or by reconstruction in water (RZn3Al-LDH). The structural data are gathered in Table 2. The XRD patterns of the powders prepared by coprecipitation reveal that the precipitation in the presence of curcumin generates the formation of a zincite-phase (ZnO , ICDD card no. 36-1451) as by-product alongside with the layered structure. In the pristine Zn3Al-LDH reference sample, the LDH is the dominant phase

and it is similar to the carbonate-intercalated Zn₃Al-LDH having a Zn/Al molar ratio of 3 standard, (Zn₃Al₂(OH)₁₆CO₃·4H₂O, ICDD card no. 38-0486). Small reflections assignable to hydrozincite, Zn₅(CO₃)₂(OH)₂, as a minor phase impurity are also observable (Zn₅(CO₃)₂(OH)₂, ICDD card no. 19-1458) (marked by * in Figure 4a). The lattice parameters are smaller for the PZnAl-CR(Aq) sample, denoting a lower Zn/Al molar ratio due to the formation of the ZnO phase. For the PZn3Al-CR(Et) solid, an extra layered phase with having a larger interlayer space has appeared, thus indicating the intercalation of larger-sized anions. Moreover, the small D₀₀₃ value obtained for this extra-phase denotes a degree of crystalline disorder along the c-axis, the axis on which the brucite-like layers are stacked.

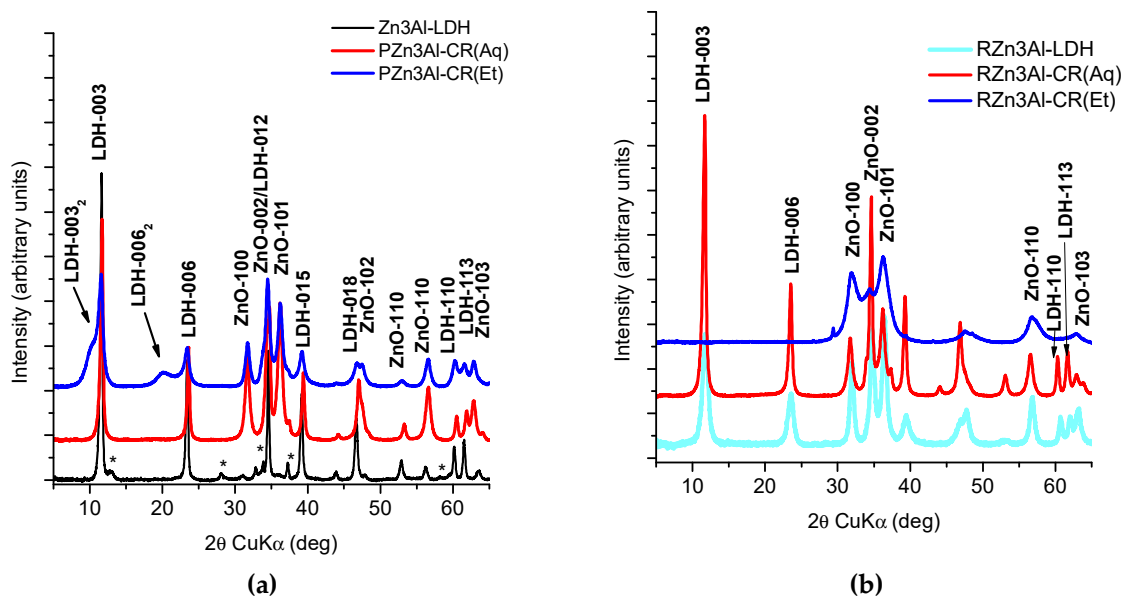


Figure 4. XRD patterns: (a) precipitated samples Zn₃Al-LDH, PZn₃Al-CR(Aq), PZn₃Al-CR(Et); (b) reconstructed samples RZn₃Al-LDH, RZn₃Al-CR(Aq), RZn₃Al-CR(Et).

Table 2. Structural data of the samples obtained from XRD analysis.

Samples	LDH Phase					ZnO Phase				
	a (Å)	c (Å)	I ₀₀₃ /I ₁₁₀	D ₁₁₀ (nm)	D ₀₀₃ (nm)	a (Å)	c (Å)	Vol (Å ³)	D (nm)	ZnO (%)
Zn ₃ Al-LDH	3.075(2)	22.9026	7.66	35.6	23.4					
RZn ₃ Al-LDH ¹	3.07(2)	22.84(7)	5.10	16.6	8.9	3.243(2)	5.183(6)	47.21	13.2	42
PZn ₃ Al-CR(Aq)	3.061(5)	22.56(4)	7.71	24.4	20.2	3.251(6)	5.21(1)	47.69	12.0	45
PZn ₃ Al-CR(Et)	3.071(6)	22.99(7)	3.37	21.9	11.9	3.262(4)	5.20(1)	47.92	11.6	22
		25.476(11)	1.34		3.9					
RZn ₃ Al-CR(Aq)	3.071(4)	22.62(5)	5.88	26.7	16.5	3.263(9)	5.21(3)	48.04	11.3	41
RZn ₃ Al-CR(Et)						3.234(2)	5.238(3)	47.44	5.3	100

¹ RZn₃Al-LDH is the structure obtained after the rehydration of CZn₃Al in water for 24 h at 25 °C.

The XRD patterns of the reconstructed samples (Figure 4b) show the partial reconstruction of the layered structure for the sample exposed to an aqueous solution. According to Kooli et al. [38], the hydration of the Zn(Al)O mixed-oxides leads to the formation of LDH with an insignificant amount of a zincite phase only for the calcined sample with a molar ratio Zn/Al=2 while, for higher Zn/Al ratios, residual ZnO is always present. The XRD pattern of the powder reconstructed in a CR ethanolic solution displays only the reflections of a ZnO-phase. The peaks are extremely broad, typically for a ZnO-phase calcined under mild conditions (400 °C–500 °C) [39]. The amount of ZnO-phase reported

to the layered LDH phases in PZn3Al-CR(Aq), PZn3Al-CR(Et) and RZn3Al-CR(Aq) fresh samples was estimated by considering the integrated intensities of the main single reflections of the ZnO-phase in RZn3Al-CR(Et) as reference. The data are included in the last column of Table 2 and disclosed values between 22 and 45% from the totality of crystalline products. However, it should also be acknowledged that the procedures used for the preparation of these powders, namely precipitation, thermal treatment and rehydration generate also amorphous oxide or hydroxides phases undetectable by XRD [38].

The reflections derived from crystalline CR were not detectable as a separate phase in the diffraction patterns of any of the CR-loaded samples. This fact may be a consequence of its dispersion as amorphous nano-particles in the inorganic matrix.

3.1.3. ATR-FTIR Characterization

The ATR-FTIR spectra of the fresh CR-containing samples are displayed in Figure 5a,b. The spectrum of the reference sample (Zn3Al-LDH) (Figure 5a) presents all the absorption bands specific to carbonate intercalated Zn₃Al-LDH at 3428 cm⁻¹ (ν -OH), 2981 cm⁻¹ (interaction of carbonate and H₂O in the interlayer through hydrogen bonds), 1630 cm⁻¹ and 772 cm⁻¹ (deformation vibrations of interlayer H₂O), 1363 cm⁻¹ (deformation vibration of carbonate anion), 770 cm⁻¹ (Al-OH out-of-plane) 617 cm⁻¹ (deformation of Zn-OH bond), 551 cm⁻¹ and 427 cm⁻¹ (vibrations in Al-O-Al and Zn-O-Zn condensed groups) [40,41].

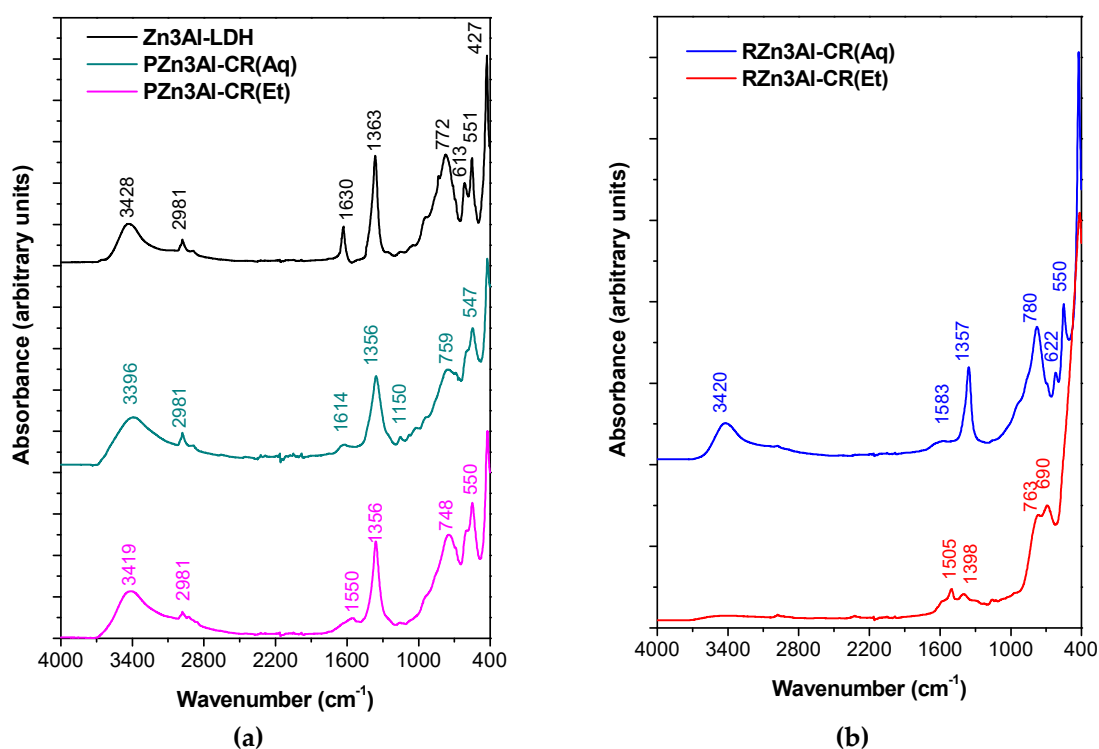


Figure 5. Normalized attenuated total reflectance (ATR)-FTIR spectra: (a) precipitated samples Zn3Al-LDH, PZn3Al-CR(Aq), PZn3Al-CR(Et); (b) reconstructed samples RZn3Al-CR(Aq), RZn3Al-CR(Et).

The spectra of CR-containing samples were similar to that of Zn3Al-LDH, except the one attributed to RZn3Al-CR(Et) (Figure 5b). In addition, the bands characteristic for neat curcumin could not be delimited from those of the LDH. However, following CR-incorporation by precipitation, the bands of the parent LDH present in the region 4000–2800 cm⁻¹ have increased their relative intensity due to the overlapping of the bands attributed to CR (see Figure 6) with those of Zn3Al-LDH (Figure 5a). There is also a noticeable red shifting of the bands at 3428 cm⁻¹, 1363 cm⁻¹ and 772 cm⁻¹ to 3396 cm⁻¹

for PZn3Al-CR(Aq), 3419 cm^{-1} for PZn3Al-CR(Et), 1356 cm^{-1} , 759 cm^{-1} for PZn3Al-CR(Aq) and 748 cm^{-1} for PZn3Al-CR(Et), respectively. The presence of the band at 1356 cm^{-1} indicates the contamination of these samples with carbonate most probably caused by the carbonation of NaOH during the manipulation before its utilization in the synthesis. This assumption is sustained by the results obtained in the analysis of carbon content presented in Table 1. In addition to that, the more pronounced asymmetry, the shifting of the bands in the region 3600–3300 cm^{-1} as well as the significant attenuation of the band corresponding to H₂O deformation vibrations at 1630 cm^{-1} compared to the reference sample Zn3Al-LDH, emphasizes the contribution of CR interactions with the inorganic matrix through hydrogen bonds. The higher intensity of the band around 550 cm^{-1} compared to the one in the region 780–748 cm^{-1} indicates an increased amount of Zn-O-Zn condensed groups in both CR-functionalized samples obtained by co-precipitation and reconstruction with CR-aqueous solution and it may be correlated with the results obtained from XRD characterization. In the spectrum of PZn3Al-CR(Aq) the band corresponding to water deformation vibrations is red shifted to 1614 cm^{-1} , indicating a perturbation in the interlayer region as a consequence of CR-incorporation, while in the spectrum of PZn3Al-CR(Et) the same band is missing. Though, a novel absorption band appears at 1550 cm^{-1} in the spectrum of PZn3Al-CR(Et) indicating the formation of a distorted Zn(II)-CR complex [42]. In the spectrum of RZn3Al-CR(Aq), the band appearing in the hydroxyl vibrations region has a lower relative intensity compared to the one of the reference material indicating a poor reconstruction due to the remaining of a segregate phase of ZnO whose presence was also confirmed by XRD. In addition to that, it was also noticed the absence of the band attributed to water deformation vibrations and the presence of a new band corresponding to Zn(II)-CR complex at 1583 cm^{-1} [42]. The spectrum of RZn3Al-CR(Et) shows five well defined absorption bands at 1505, 1398, 763, 680 and 427 cm^{-1} . Among these bands, the one at 1505 cm^{-1} is correlated to the most intense band of curcumin (Figure 6), the band at 1398 cm^{-1} could be assimilated to a red shift of the curcumin band at 1427 cm^{-1} while the band at 680 cm^{-1} could be also due to a red shift of the curcumin band at 808 cm^{-1} . The bands at 763 and 427 cm^{-1} are related to M-O vibration modes [40,41]. The absence of the band at ca. 3400 cm^{-1} in this spectrum shows the absence of the reconstruction effect.

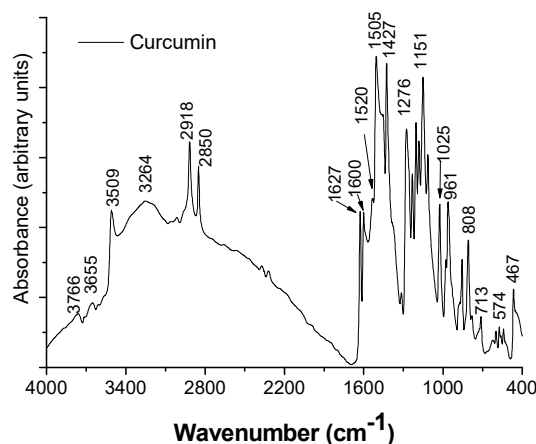


Figure 6. ATR-FTIR spectrum of the neat curcumin (CR) utilized in this study.

3.1.4. DR-UV-Vis Characterization

The DR-UV-Vis spectra of CR-containing samples along with the spectrum of CR are displayed in Figure 7a,b.

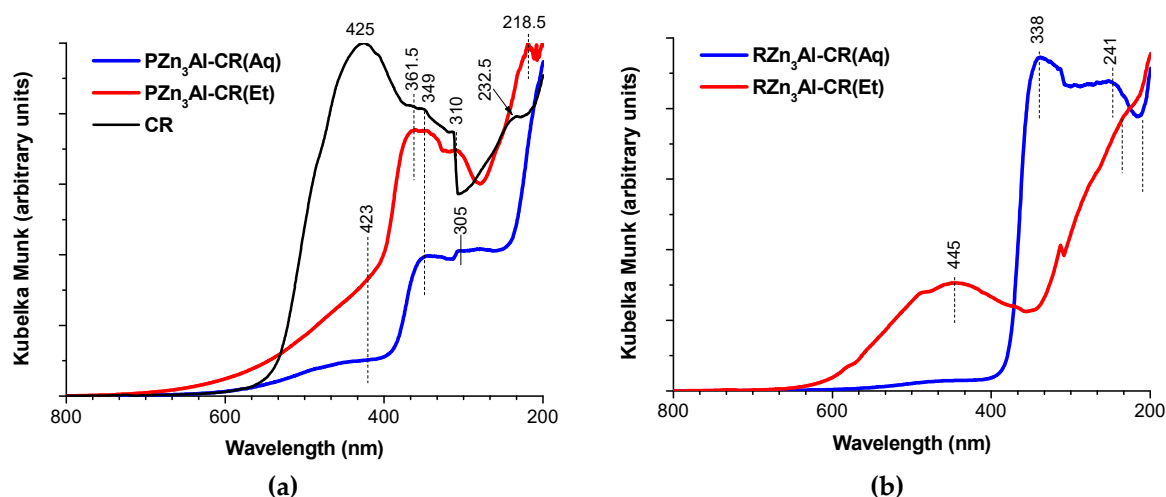


Figure 7. Diffuse reflectance (DR)-UV-Vis spectra: (a) neat curcumin (CR) and precipitated samples, PZn₃Al-CR(Aq), PZn₃Al-CR(Et); (b) reconstructed samples RZn₃Al-CR(Aq), RZn₃Al-CR(Et).

The spectrum of the neat curcumin powder has the highest intensity absorption band in the visible region at 425 nm. This band is shifted to 455 nm and is clearly evidenced only in the spectrum of the sample RZn₃Al-CR(Et) which shows also the second absorption band specific to CR at 364 nm. Meanwhile, in the spectra of the precipitated samples PZn₃Al-CR(Aq) and PZn₃Al-CR(Et) the maximum absorption in the visible domain appears at 361.5 and 349 nm, respectively and only an inflection of the absorption curve is noticed at 423 nm. The absorption maxima observed in these two spectra indicate that during the preparation of the samples curcumin was partially decomposed to a mixture of feruloyl methane and ferulic acid whose most intense absorption peaks are at 340 nm, and 305 nm respectively [43]. In the spectrum of RZn₃Al-CR(Aq), only the characteristic absorption bands for feruloyl methane at 340 nm and 241 nm were noticed.

3.2. Curcumin Release Studies

The results of the CR-release studies performed by contacting the synthesized solids with different buffer solutions (pH 1, pH 2, pH 5, pH 7 and pH 8) at 25 °C during 24 h under mild stirring are presented in Figure 8a–d. The release of curcumin from pure curcumin powder into the same buffer solutions was determined using an amount of curcumin powder equal to the average amount of curcumin incorporated in 0.5 g of the LDH samples (e.g., 56.25 mg) which was immersed in 50 mL of buffer solution. The results obtained under operating conditions (temperature, stirring and duration) similar to those employed for CR-containing LDH samples are presented in Figure 9.

The results displayed in Figure 8 indicate that for all samples the release of curcumin was favored at lower pH values and was almost insignificant at pH values higher than 5. It is also noticeable that CR-loaded samples prepared with ethanolic solutions were able to release higher amounts of CR than the samples prepared with aqueous solutions. At each pH value, the amount of curcumin released in the buffer solutions varied in the order: RZn₃Al-CR(Et) > PZn₃Al-CR(Et) > PZn₃Al-CR(Aq) > RZn₃Al-CR(Aq). At pH 1, CR was released faster from RZn₃Al-CR(Et) since half of the total amount of released curcumin was reached after 2 h, while for the other solids only about one third of the total amount was reached in that period. Under similar conditions, the results plotted in Figure 9 show that the pH decrease led also to an increased release of curcumin from pure curcumin powder into the buffer solutions, but the highest value obtained was lower than 0.8%. When the release tests with pure curcumin powder were performed during 4 h at 37 °C (the physiological temperature) the amount of released CR varied in the order: 1.0 ± 0.1% at pH 1, 0.8 ± 0.1% at pH 2, 0.5 ± 0.1% at pH 5, 0.4 ± 0.1% at pH 7 and 0.3 ± 0.1% at pH 8. The effect of the

temperature on the CR-release after 4 h from the sample RZn3Al-CR(Et) was also not significant as it may be seen from the results plotted in Figure 10.

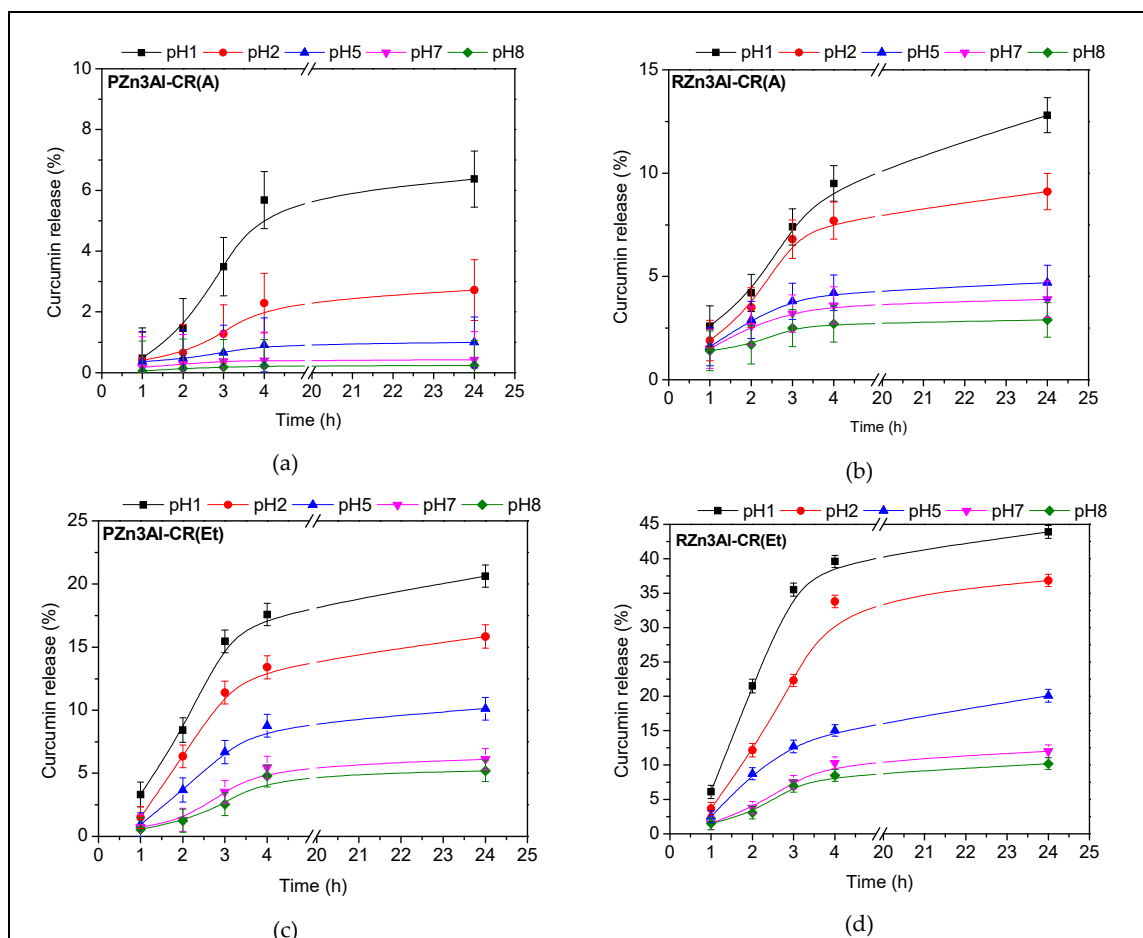


Figure 8. Curcumin release from the solid samples during 24 h in different pH buffers: (a) PZn3Al-CR(Aq); (b) RZn3Al-CR(Aq); (c) PZn3Al-CR(Et); (d) RZn3Al-CR(Et).

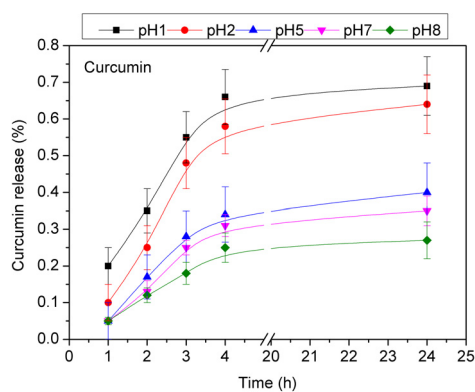


Figure 9. Curcumin release from pure curcumin powder.

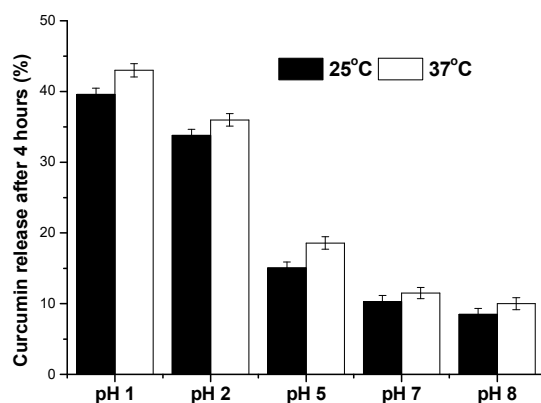


Figure 10. Curcumin release from RZn3Al-CR(Et) in different buffer solutions at 25 and 37 °C.

The solid samples recovered after each CR-release test were analyzed by DR-UV-Vis spectroscopy and the spectra are presented in Figure 11a–d.

The alteration of the spectra of the samples after they were contacted with different buffered solutions indicates how the chemical composition of each buffer affected the CR-functionalized solids. After the tests performed at pH 7 and pH 8 in buffered solutions containing potassium dihydrogen phosphate/di-sodium hydrogen phosphate, and potassium dihydrogen phosphate/sodium hydroxide, respectively, none of the specific absorption bands observed in the spectra of the fresh samples could be noticed. This fact suggests the occurrence of chemical reactions between the components of the buffer and the solid leading to the decomposition of the chemical species responsible for the absorption bands noticed in the DR-UV-Vis spectra of the fresh samples. After the tests performed in acid buffers at pH 1 and 2, the main bands specific to the fresh solids were preserved but their relative intensity compared to the spectra of the fresh solids decreased, suggesting that a partial dissolution of the inorganic host took place. In addition to that, for the samples PZn3Al-CR(Aq), PZn3Al-CR(Et) and RZn3Al-CR(Aq) their position was shifted to lower wavelengths. The decrease was more intense at pH 1 when the highest amount of curcumin was released for each sample. The contact of the CR-loaded solids with the pH 5 buffer solution containing citric acid and sodium hydroxide affected all the samples. In the spectra of the samples prepared with CR-ethanolic solution (Figure 11b,d), after the contact with pH 5 buffer, the absorption maximum characteristic to bicyclopentadione at 232 nm was noticed [43]. This maximum was also noticeable as a shoulder in the spectrum of PZn3Al-CR(Aq) (Figure 11a), but it was absent in the spectrum of RZn3Al-CR(Aq) (Figure 11c).

The interactions between the CR-containing samples and different buffer solutions were also evidenced in the ATR-FTIR spectra of the solids recovered after the CR-release tests performed with each buffer solution which are presented in Figure 12.

The spectra of all the samples recovered from the alkaline buffer solutions (pH 7 and 8) have the main absorption bands around 1000 cm^{-1} (marked with * in Figure 12) and they were attributed to the phosphate anion which was intensely adsorbed on the solids. In this case, the spectra of the two samples prepared by co-precipitation (Figure 12a,b) presented the same absorption maxima, whereas in the spectra of the samples RZn3Al-CR(Aq) and RZn3Al-CR(Et) recovered from pH 8 buffer solution, the band corresponding to water bending at 1620 cm^{-1} was absent. The spectra of the samples recovered from acid buffer solutions (pH 1, pH 2 and pH 5, respectively) were mostly altered in the mid-infrared region $1600\text{--}1300\text{ cm}^{-1}$ (delimited by a dashed rectangle in Figure 10) where the bands specific to citrate occur ($\nu_{\text{as}}(\text{COO}^-)$ at 1612 cm^{-1} ; $\nu_{\text{s}}(\text{COO}^-)$ at 1396 cm^{-1} , $\delta_{(\text{CH}_2)}$ at 1365 cm^{-1} [44]). For the precipitated samples (Figure 12a,b) the relative intensity of the band around 1600 cm^{-1} was sensibly higher than in the spectra of the fresh samples, while for the reconstructed ones, the relative intensity of all the bands in the domain $1600\text{--}1300\text{ cm}^{-1}$ was definitely increased compared to the spectra of the fresh samples (Figure 12c,d) indicating that citrate was better adsorbed on the surface of the reconstructed solids.

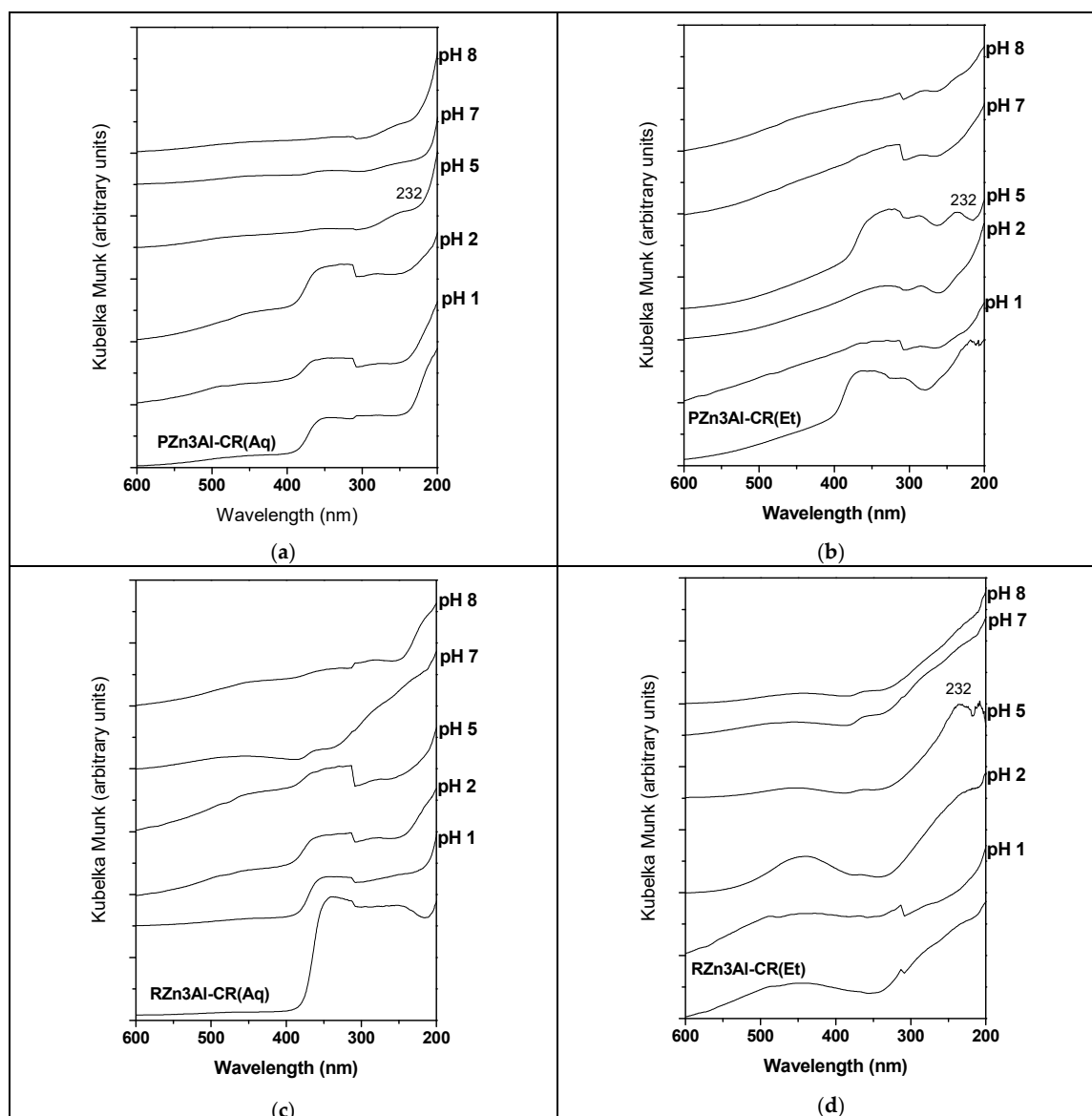


Figure 11. DR-UV-Vis spectra of the CR-containing samples after the CR-release tests at different pH values: (a) PZn3Al-CR(Aq); (b) RZn3Al-CR(Aq); (c) PZn3Al-CR(Et); (d) RZn3Al-CR(Et).

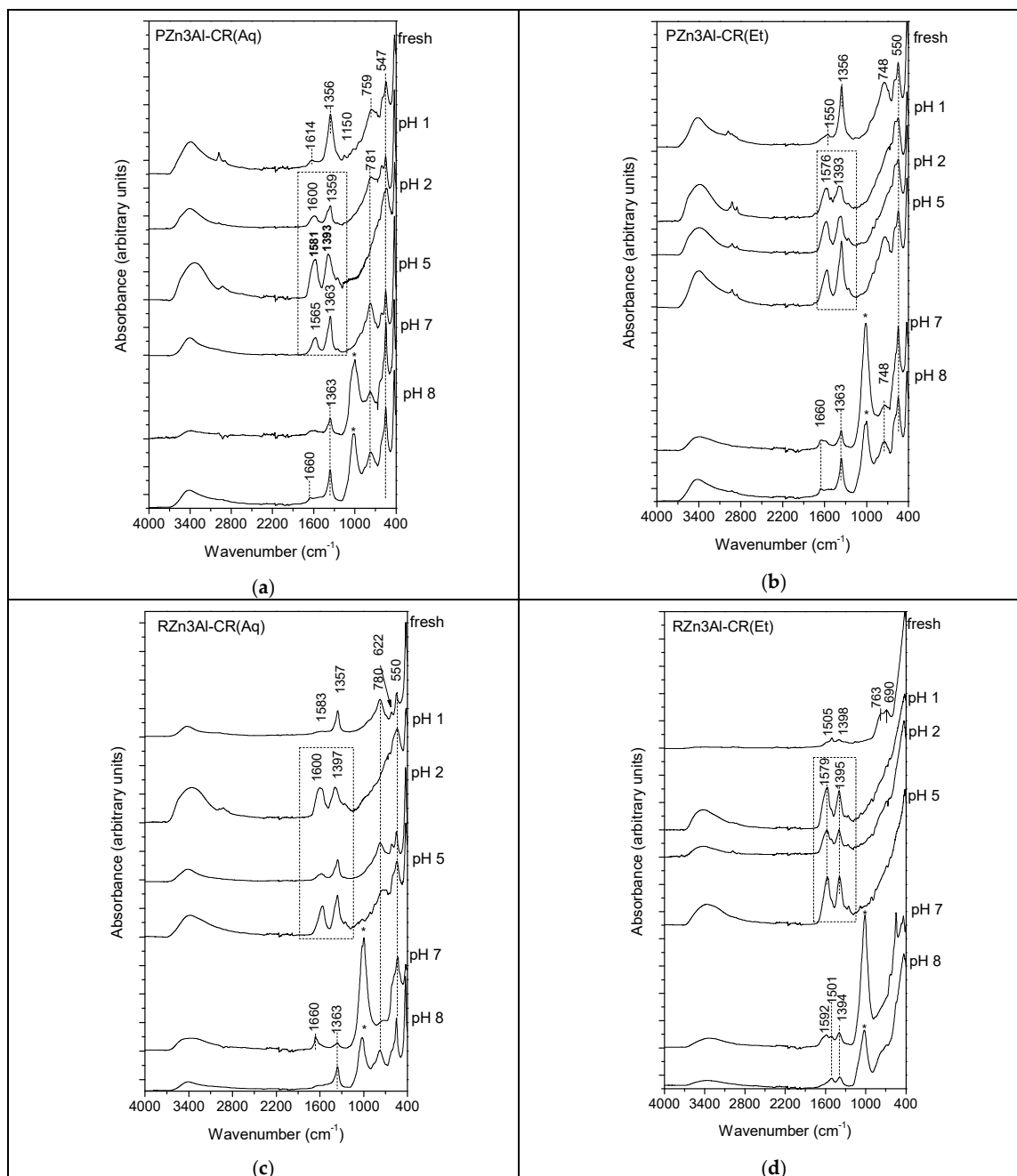


Figure 12. ATR-FTIR spectra of the CR-containing samples after the CR-release tests at different pH values: (a) PZn3Al-CR(Aq); (b) RZn3Al-CR(Aq); (c) PZn3Al-CR(Et); (d) RZn3Al-CR(Et).

4. Discussion

The investigation of the collected data has revealed a contradiction between the results of the chemical analysis concerning the curcumin content in the samples and those of the other characterizations which did not clearly indicate the presence of CR in the solids except the one obtained by reconstruction with CR-ethanolic solution (RZn3Al-CR(Et)). A possible explanation for this inconsistency is revolving around the CR-loading present in the solids, which was calculated based on the determination of the total organic carbon content, including also the carbon from the compounds obtained by the degradation of curcumin during the syntheses performed at basic pH. Several studies concerning the stability of curcumin in the alkaline medium have suggested that the degradation products are ferulic acid, feruloyl methane, vanillin and

trans-6-(4'-hydroxy-3'-methoxyphenyl)-2,4-dioxo-5-hexenal [2,7,8,43,44]. The results of our DR-UV-Vis analysis (Figure 7) confirmed the presence of feruloyl methane and ferulic acid in the samples obtained by co-precipitation PZn3Al-CR(Aq), PZn3Al-CR(Et), while in the sample RZn3Al-CR(Aq) only the presence of feruloyl methane was evidenced. This fact implies that when curcumin is contacted with an aqueous solution containing NaOH, the main degradation product resulted is feruloyl methane and that ferulic acid is obtained most probably during the ageing of the precipitates. Our findings are in agreement with those of Gordon and Schneider [43], which showed that vanillin and ferulic acid were not the major degradation products of curcumin.

From the results of DR-UV-Vis, it could also be inferred that the degradation of curcumin was less pronounced when the co-precipitation was performed with CR-ethanolic solution since the spectrum of PZn3Al-CR(Et) showed a more intense absorption in the region 400–600 nm compared to the spectrum of PZn3Al-CR(Aq). This fact could be due to the formation of a CR-Zn(II) complex which according to literature data has the maximum absorption in the visible region at 455 nm [42]. The presence of such a complex was also suggested by the ATR-FTIR spectrum of PZn3Al-CR(Et) (Figure 5a) displaying an absorption maximum at 1550 cm^{-1} . The red shifting of the absorption maximum specific to CR-Zn(II) complex from 1583 cm^{-1} [42] to 1550 cm^{-1} , could be related to its distortion under the influence of the LDH matrix and/or to its participation as secondary layered phase (whose presence was indicated by XRD analysis) in the LDH structure. The ATR-FTIR spectrum of the sample RZn3Al-CR(Aq) (Figure 5b) showed a sensibly weaker absorption band specific to CR-Zn(II) confirming that the stabilization of curcumin by complexation with Zn(II) was much lower in this case, most probably due to its degradation during the dissolution in the aqueous alkaline solution. The degradation of curcumin during the co-precipitation and reconstruction with alkaline aqueous CR-solution could also explain why the XRD patterns of the samples PZn3Al-CR(Aq) and RZn3Al-CR(Aq) did not show the specific diffraction lines of CR. The lower degradation of CR during the preparation of the PZn3Al-CR(Et) solid accompanied by the formation of the CR-Zn(II) complex evidenced by ATR-FTIR could be responsible for the obtaining of the extra layered phase with slightly larger interlayer space and a degree of crystalline disorder along the *c*-axis revealed by the XRD analysis (Figure 4a). Even if both ATR-FTIR and DR-UV-Vis spectra of the sample RZn3Al-CR(Et) obtained by reconstruction with CR-ethanolic solution indicated the presence of curcumin, its presence was not evidenced as a single phase in the XRD pattern most probably because nano-particles of curcumin were dispersed on the surface of this solid which contained also nano-sized particles of ZnO (see Table 2). Considering the results of the characterization studies it may be concluded that curcumin was incorporated without degradation only in RZn3Al-CR(Et), while in the rest of the solids, CR-Zn(II) complex and different degradation products of curcumin were incorporated in various extents. The amount of curcumin released from the synthesized solids was higher for those prepared with CR-ethanolic solutions (e.g., RZn3Al-CR(Et) and PZn3Al-CR(Et)) (Figure 8) and was well correlated to the content of the stabilized curcumin in the samples.

The release of curcumin from the CR-loaded solids was significantly influenced by the pH of the buffer solution utilized in the “in vitro” release studies. The buffers with acid pH (1, 2 and 5) allowed a better release of curcumin than the neutral to basic pH buffers (pH 7 and 8) which have a significant degrading effect on curcumin as it was indicated by Wang et al. [45]. This fact suggests that curcumin will be better released in the stomach where the pH can vary in the range 1.5–6.5 (e.g., pH 1.5–4.0 in the lower portion of the stomach and pH 4.0–6.5 in the upper portion of the stomach where predigestion takes place), than in the duodenum where the pH changes from 7.0 to 8.5 [46,47]. Considering the results of the CR-release tests (Figure 8) it may be inferred that CR-release will be lower in the upper portion of the stomach where the pH is less acidic (release tests at pH 5) and will enhance gradually as the solid will reach the lower portion of the stomach (release tests at pH 2 and pH 1), and it will be negligible when the solid reaches the duodenum (release tests at pH 7 and pH 8).

5. Conclusions

Our studies showed that the incorporation of curcumin into a Zn₃Al-LDH structure can be achieved by co-precipitation only if the curcumin is utilized as an ethanolic solution. However, since the co-precipitation is performed with NaOH for pH adjustment, the partial degradation of curcumin could not be avoided. Hence the curcumin release capacity of this sample (PZn₃Al-Cr(ET)) under acid pH conditions was by 20% lower than that of the sample prepared by reconstruction RZn₃Al-CR(Et) even if the CR-concentration in the fresh samples was not significantly different (9.3 and 11.5 wt. %, respectively). The utilization of alkaline CR-aqueous solution either in the co-precipitation or in the reconstruction method leads to the obtaining of a Zn₃Al-LDH structure impurified by ZnO phase where amorphous curcumin and mostly its degradation products were spread flatly on the surface of the inorganic matrix and at the edges of the layers. Taking into account both the results of the characterizations and those of CR-release tests, the preferable method to obtain CR-loaded Zn₃Al solids from LDH precursors is the so-called “reconstruction” (since it does not restore the layered LDH structure) with CR-ethanolic solution which does not allow curcumin degradation and ensures also the highest curcumin release from the solid. Therefore, the sample RZn₃Al-CR(Et) was the one selected for future antimicrobial activity tests.

Author Contributions: Conceptualization, R.Z.; formal analysis, E.B. and R.B.; investigation, O.D.P., A.Ş. and R.Z.; methodology, O.D.P. and R.Z.; project administration, O.D.P.; visualization, O.D.P.; writing—original draft, A.Ş. and R.Z.; writing—review and editing, R.Z. All authors have read and agreed to the published version of the manuscript.

Funding: This research was funded by the Romanian Ministry of Research and Innovation, CCCDI-UEFISCDI, grant number PN-III-P1-1.2-PCCDI-2017-0387/80PCCDI, within PNCDI III program.

Conflicts of Interest: The authors declare no conflict of interest.

References

1. Aggarwal, S.; Ichikawa, H.; Takada, Y.; Sandur, S.K.; Shishodia, S.; Aggarwal, B.B. Curcumin (diferuloylmethane) down-regulates expression of cell proliferation and antiapoptotic and metastatic gene products through suppression of IkappaBalpha kinase and Akt activation. *Mol. Pharmacol.* **2006**, *69*, 195–206. [[CrossRef](#)] [[PubMed](#)]
2. Heger, M.; van Golen, R.F.; Broekgaarden, M.; Michel, M.C. The molecular basis for the pharmacokinetics and pharmacodynamics of curcumin and its metabolites in relation to cancer. *Pharmacol. Rev.* **2014**, *66*, 222–307. [[CrossRef](#)] [[PubMed](#)]
3. Pulido-Moran, M.; Moreno-Fernandez, J.; Ramirez-Tortosa, C.; Ramirez-Tortosa, M.C. Curcumin and Health. *Molecules* **2016**, *21*, 264. [[CrossRef](#)] [[PubMed](#)]
4. Priyadarsini, K.I.; Maity, D.K.; Naik, G.H.; Kumar, M.S.; Unnikrishnan, M.K.; Satav, J.G.; Mohan, H. Role of phenolic O-H and methylene hydrogen on the free radical reactions and antioxidant activity of curcumin. *Free Radic. Biol. Med.* **2003**, *35*, 475–484. [[CrossRef](#)]
5. Kolev, T.M.; Velcheva, E.A.; Stamboliyska, B.A.; Spiteller, M. DFT and Experimental Studies of the Structure and Vibrational Spectra of Curcumin. *Int. J. Quantum Chem.* **2005**, *102*, 1069–1079. [[CrossRef](#)]
6. Jovanovic, S.V.; Steenken, S.; Boone, C.W.; Simic, M.G. H-Atom Transfer is a Preferred Antioxidant Mechanism of Curcumin. *J. Am. Chem. Soc.* **1999**, *121*, 9677–9681. [[CrossRef](#)]
7. Jagannathan, R.; Abraham, P.M.; Poddar, P. Temperature-Dependent Spectroscopic Evidences of Curcumin in Aqueous Medium: A Mechanistic Study of Its Solubility and Stability. *J. Phys. Chem. B* **2012**, *116*, 14533–14540. [[CrossRef](#)]
8. Tønnesen, H.H.; Másson, M.; Loftsson, T. Studies of curcumin and curcuminoids. XXVII. Cyclodextrin complexation: Solubility, chemical and photochemical stability. *Int. J. Pharm.* **2002**, *244*, 127–135. [[CrossRef](#)]
9. Parvathy, K.S.; Negi, P.S.; Srinivas, P. Antioxidant, antimutagenic and antibacterial activities of curcumin-β-diglycoside. *Food Chem.* **2009**, *115*, 265–271. [[CrossRef](#)]
10. Sneharani, A.H.; Singh, S.A.; Appu Rao, A.G. Interaction of αS1-Casein with Curcumin and Its Biological Implications. *J. Agric. Food Chem.* **2009**, *57*, 10386–10391. [[CrossRef](#)]

11. Sneharani, A.H.; Karakkat, J.V.; Singh, S.A.; Appu Rao, A.G. Interaction of Curcumin with β -Lactoglobulin—Stability, Spectroscopic Analysis, and Molecular Modeling of the Complex. *J. Agric. Food Chem.* **2010**, *58*, 11130–11139. [[CrossRef](#)] [[PubMed](#)]
12. Bisht, S.; Feldmann, G.; Soni, S.; Ravi, R.; Karikar, C.; Maitra, A.M.; Maitra, A.N. Polymeric nanoparticle encapsulated curcumin (“nanocurcumin”): A novel strategy for human cancer therapy. *J. Nanobiotechnol.* **2007**, *5*, 3. [[CrossRef](#)] [[PubMed](#)]
13. Tiwari, S.K.; Agarwal, S.; Seth, B.; Yadav, A.; Nair, S.; Bhatnagar, P.; Karmakar, M.; Kumari, M.; Chauhan, L.K.; Patel, D.K.; et al. Curcumin-loaded nanoparticles potently induce adult neurogenesis and reverse cognitive deficits in Alzheimer’s disease model via canonical Wnt/b-catenin pathway. *ACS Nano* **2014**, *8*, 76–103. [[CrossRef](#)] [[PubMed](#)]
14. Sun, D.; Zhuang, X.; Xiang, X.; Liu, Y.; Zhang, S.; Liu, C.; Barnes, S.; Grizzle, W.; Miller, D.; Zhang, H.G. A novel nanoparticle drug delivery system: The anti-inflammatory activity of curcumin is enhanced when encapsulated in exosomes. *Mol. Ther.* **2010**, *18*, 1606–1614. [[CrossRef](#)]
15. Wang, W.; Zhu, R.; Xie, Q.; Li, A.; Xiao, Y.; Li, K.; Liu, H.; Cui, D.; Chen, Y.; Wang, S. Enhanced bioavailability and efficiency of curcumin for the treatment of asthma by its formulation in solid lipid nanoparticles. *Int. J. NanoMed.* **2012**, *7*, 3667–3677. [[CrossRef](#)]
16. Gonçalves, C.; Pereira, P.; Schellenberg, P.; Coutinho, P.J.; Gama, F.M. Self-assembled dextrin nanogel as curcumin delivery system. *J. Biomater. Nanobiotechnol.* **2012**, *3*, 178–184. [[CrossRef](#)]
17. Falconieri, M.C.; Adamo, M.; Monasterolo, C.; Bergonzi, M.C.; Coronello, M.; Bilia, A.R. New dendrimer based nanoparticles enhance curcumin solubility. *Planta Med.* **2017**, *83*, 420–425. [[CrossRef](#)]
18. Shome, S.; Talukdar, A.D.; Choudhury, M.D.; Bhattacharya, M.K.; Upadhyaya, H. Curcumin as potential therapeutic natural product: A nanobiotechnological perspective. *J. Pharm. Pharmacol.* **2016**, *68*, 1481–1500. [[CrossRef](#)]
19. Zebib, B.; Mouloungui, Z.; Noirot, V. Stabilization of Curcumin by Complexation with Divalent Cations in Glycerol/Water System. *Bioinorg. Chem. Appl.* **2010**, *2010*, 292760. [[CrossRef](#)]
20. Jiang, T.; Wang, L.; Zhang, S.; Sun, P.C.; Ding, C.F.; Chu, Y.Q.; Zhou, P. Interaction of curcumin with Al (III) and its complex structures based on experiments and theoretical calculations. *J. Mol. Struct.* **2011**, *1004*, 163–173. [[CrossRef](#)]
21. Cavani, F.; Trifirò, F.; Vaccari, A. Hydrotalcite-type anionic clays: Preparation, properties and applications. *Catal. Today* **1991**, *11*, 173–301. [[CrossRef](#)]
22. Trifiro, F.; Vaccari, A. Hydrotalcite-like Anionic Clays (Layered Double Hydroxides). In *Comprehensive Supramolecular Chemistry*; Atwood, J.L., Davies, J.E.D., MacNicol, D.D., Vögtle, F., Eds.; Pergamon: Oxford, UK, 1996; Volume 7, pp. 251–291.
23. Isupov, V.P.; Chupakhina, L.E.; Mitrofanova, R.P. Mechanochemical synthesis of double hydroxides. *J. Mater. Synth. Process.* **2000**, *8*, 251–253. [[CrossRef](#)]
24. Richetta, M.; Medaglia, P.G.; Mattoccia, A.; Varone, A.; Pizzoferrato, R. Layered Double Hydroxides: Tailoring Interlamellar Nanospace for a Vast Field of Applications. *J. Mater. Sci. Eng.* **2017**, *6*, 360. [[CrossRef](#)]
25. Choy, J.H.; Jung, J.S.; Oh, J.M.; Park, M.; Jeong, J.; Kang, Y.K.; Han, O.J. Layered double hydroxide as an efficient drug reservoir for folate derivatives. *Biomaterials* **2004**, *25*, 3059–3064. [[CrossRef](#)] [[PubMed](#)]
26. Gordijo, C.R.; Barbosa, C.A.S.; Ferreira, A.M.D.C.; Constantino, V.R.L.; Silva, D.D. Immobilization of ibuprofen and copper-ibuprofen drugs on layered double hydroxides. *J. Pharm. Sci.* **2005**, *94*, 1135–1148. [[CrossRef](#)] [[PubMed](#)]
27. Costantino, U.; Ambroggi, V.; Nocchetti, M.; Perioli, L. Hydrotalcite-like compounds: Versatile layered hosts of molecular anions with biological activity. *Microporous Mesoporous Mater.* **2008**, *107*, 149–160. [[CrossRef](#)]
28. Oh, J.-M.; Park, M.; Kim, S.-T.; Jung, J.-Y.; Kang, Y.-G.; Choy, J.-H. Efficient delivery of anticancer drug MTX through MTX-LDH nanohybrid system. *J. Phys. Chem. Solids* **2006**, *67*, 1024–1027. [[CrossRef](#)]
29. Bi, X.; Zhang, H.; Dou, L. Layered Double Hydroxide-Based Nanocarriers for Drug Delivery. *Pharmaceutics* **2014**, *6*, 298–332. [[CrossRef](#)]
30. Muráth, S.; Szerlauth, A.; Sebók, D.; Szilágyi, I. Layered Double Hydroxide Nanoparticles to Overcome the Hydrophobicity of Ellagic Acid: An Antioxidant Hybrid Material. *Antioxidants* **2020**, *9*, 153. [[CrossRef](#)]
31. Muráth, S.; Alsharif, N.B.; Sáring, S.; Katana, B.; Somosi, Z.; Szilágyi, I. Antioxidant Materials Based on 2D Nanostructures: A Review on Recent Progresses. *Crystals* **2020**, *10*, 148. [[CrossRef](#)]

32. Wang, Q.; O'Hare, D. Recent Advances in the Synthesis and Application of Layered Double Hydroxide (LDH) Nanosheets. *Chem. Rev.* **2012**, *112*, 4124–4155. [CrossRef]
33. Supun Samindra, K.M.; Kottegoda, N. Encapsulation of curcumin into layered double hydroxides. *Nanotechnol. Rev.* **2014**, *3*, 579–589. [CrossRef]
34. Megalathan, A.; Kumarage, S.; Dilhari, A.; Weerasekera, M.M.; Samarasinghe, S.; Kottegoda, N. Natural curcuminoids encapsulated in layered double hydroxides: A novel antimicrobial nanohybrid. *Chem. Cent. J.* **2016**, *10*, 35. [CrossRef]
35. Gayani, B.; Dilhari, A.; Wijesinghe, G.K.; Kumarage, S.; Abayaweera, G.; Samarakoon, S.R.; Perera, I.C.; Kottegoda, N.; Weerasekera, M.M. Effect of natural curcuminoids-intercalated layered double hydroxide nanohybrid against *Staphylococcus aureus*, *Pseudomonas aeruginosa*, and *Enterococcus faecalis*: A bactericidal, antibiofilm, and mechanistic study. *MicrobiologyOpen* **2019**, *8*, e723. [CrossRef] [PubMed]
36. Król, A.; Pomastowski, P.; Rafińska, K.; Railean-Plugaru, V.; Buszewski, B. Zinc oxide nanoparticles: Synthesis, antiseptic activity and toxicity mechanism. *Adv. Colloid Interface Sci.* **2017**, *249*, 37–52. [CrossRef]
37. Zăvoianu, R.; Pavel, O.D.; Cruceanu, A.; Florea, M.; Bîrjega, R. Functional layered double hydroxides and their catalytic activity for 1,4-addition of n-octanol to 2-propenonitrile. *Appl. Clay Sci.* **2017**, *146*, 411–422. [CrossRef]
38. Kooli, E.; Depège, C.; Ennaqadi, A.; De Roy, A.; Besse, J.E. Rehydration of Zn-Al layered double hydroxides. *Clays Clay Miner.* **1997**, *45*, 92–98. [CrossRef]
39. Elhalil, A.; Farnane, M.; Machrouhi, A.; Mahjoubi, F.Z.; Elmoubarki, R.; Tounsadi, H.; Abdennouri, M.; Barka, N. Effects of molar ratio and calcination temperature on the adsorption performance of Zn/Al layered double hydroxide nanoparticles in the removal of pharmaceutical pollutants. *J. Sci. Adv. Mater. Devices* **2018**, *3*, 188–195. [CrossRef]
40. Karami, Z.; Aghazadeh, M.; Jouyandeh, M.; Zarrintaj, P.; Vahabi, H.; Ganjalnia, M.R.; Torre, L.; Puglia, D.; Sae, M.R. Epoxy/Zn-Al-CO₃ LDH nanocomposites: Curability assessment. *Prog. Org. Coat.* **2020**, *138*, 105355. [CrossRef]
41. George, G.; Saravanakumar, M.P. Facile synthesis of carbon-coated layered double hydroxide and its comparative characterisation with Zn–Al LDH: Application on crystal violet and malachite green dye adsorption—Isotherm, kinetics and Box-Behnken design. *Environ. Sci. Pollut. Res.* **2018**, *25*, 30236–30254. [CrossRef]
42. Zhao, X.Z.; Jiang, T.; Wang, L.; Yang, H.; Zhang, S.; Zhou, P. Interaction of curcumin with Zn (II) and Cu (II) ions based on experiment and theoretical calculation. *J. Mol. Struct.* **2010**, *984*, 316–325. [CrossRef]
43. Gordon, O.N.; Schneider, C. Vanillin and ferulic acid: Not the major degradation products of curcumin. *Trends Mol. Med.* **2012**, *18*, 361–363. [CrossRef] [PubMed]
44. Silva, A.M.N.; Kong, X.; Parkin, M.C.; Cammack, R.; Hider, R.C. Iron (III) citrate speciation in aqueous solution. *Dalton Trans.* **2009**, *40*, 8616–8625. [CrossRef] [PubMed]
45. Wang, Y.J.; Pan, M.H.; Cheng, A.L.; Lin, L.I.; Ho, Y.S.; Hsieh, C.Y.; Lin, J.K. Stability of curcumin in buffer solutions and characterization of its degradation products. *J. Pharm. BioMed. Anal.* **1997**, *15*, 1867–1876. [CrossRef]
46. Allegany Nutrition. The Enzyme Specialists. Available online: <https://www.alleganynutrition.com/supporting-pages/the-human-digestive-tract-ph-range-diagram/> (accessed on 1 February 2020).
47. Beasley, D.E.; Koltz, A.M.; Lambert, J.E.; Fierer, N.; Dunn, R.R. The evolution of stomach acidity and its relevance to the Human Microbiome. *PLoS ONE* **2015**, *10*, e0134116. [CrossRef] [PubMed]

